

Investigating the Interplay Between Spin-Vibrational Coupling and Blocking Temperature in Designing High-Performance Pseudo D_{5h} Dy(III) Single Ion Magnets

Sourav Dey, Tanu Sharma and Gopalan Rajaraman*

Department of Chemistry, Indian Institute of Technology Bombay, Mumbai, Powai-400076.
India. Email: rajaraman@chem.iitb.ac.in

Abstract: At the cutting edge of high-performance single-molecule magnets (SMMs) lie lanthanide-based complexes, renowned for their potent magnetic anisotropy. The performance of the SMMs is measured generally via the barrier height for magnetization reversal (U_{eff}) and blocking temperature (T_B), below which the magnetization is fully frozen. To enhance the U_{eff} and T_B values in lanthanide-based SMMs, the static crystal field splitting of m_J levels has been effectively adjusted through ligand design, leveraging the oblate/prolate ground state 4f electron density shape. However, the maximum fine-tuning that can be achieved via ligand design called the axial limit is already reached in this class of compounds and demand new design principle to enhance the SMM characteristics to suit end-user applications. Among other avenues that can be explored to improve the SMM characteristics, a deeper understanding of spin-phonon coupling, critical to advancing T_B values, offers numerous advantages. However, there are only a handful of examples where this is deciphered. In this work, using a combination of DFT and *ab initio* CASSCF calculations, we have performed spin-phonon calculations of five classes of pseudo D_{5h} Dy(III) SIMs exhibiting T_B value in the range of 4.5 K to 36 K ([Dy(bbpen)Br] (**1**, $H_2bbpen=N,N'$ -bis(2-hydroxybenzyl)- N,N' -bis(2-methylpyridyl)ethylenediamine), [Dy(OCMe₃)Br(THF)₅][BPh₄] (**2**) [Dy(OSiMe₃)Br(THF)₅][BPh₄] (**3**), [Dy(L^{N5})(Ph₃SiO)₂](BPh₄).CH₂Cl₂ (**4**) and [L₂Dy(H₂O)₅][I]₃.L₂.H₂O (**5**, L = ^tBuPO(NHⁱPr)₂). The approach provided here not only reduces the computational cost but also suggests chemical intuition to improve the performance of this class of compounds. Our calculations reveal that low-energy vibrational modes govern the magnetization relaxation in these SIMs. A flexible first coordination sphere found on some of the complexes was found to be responsible for low-energy vibrations that flip the magnetization reducing the T_B values drastically (complexes **2** and **3**). On the other hand, a rigid first coordination sphere and a stiff ligand framework move the spin-vibrational coupling that causes the relaxation to lie beyond the secondary coordination sphere resulting in the increase of T_B values. Learning from this exercise, we have undertaken several *in silico* models based on these vibrations to improvise the T_B values. Some of these predictions were correlated to literature precedents, offering confidence in the methodology employed. To this end, our comprehensive investigation, involving twenty-three molecules/models and five sets of geometries for the pseudo D_{5h} Dy(III) single-ion magnets (SIMs), unveils a treasure trove of chemically sound design clues, poised to enhance the T_B values in this fascinating molecular realm.

1. Introduction

Single-Molecule Magnets (SMMs) are nanoscale molecule-based magnets exhibiting permanent magnetization similar to bulk magnets opening up the bottom-up approach to molecule-based devices such as new generation of information storage devices, solid-state Q-bits for quantum computing and spintronics devices. To employ these molecules in end-user applications, magnetic relaxation time (τ), the timescale in which an SMM preserve its magnetization, and blocking temperature (T_B) below which the magnetization is fully frozen need to be improved.¹⁻⁹ Further, the molecule should be stable under ambient conditions for the fabrication process to realize the potential applications proposed. While early SMMs based on transition metal clusters yielded T_B values in the range of liquid helium temperatures, the advent of lanthanide-based SMMs significantly improved T_B values.¹⁰⁻¹² The first mononuclear lanthanide-based SMM (also called SIM), $[\text{TbPc}_2]^-$ (Pc = phthalocyanine), was discovered in 2003 and is reported to have a T_B value of 1.7 K and U_{eff} of 230 cm^{-1} .¹³ Thereafter, many lanthanide-based SMMs have been reported till 2015, but the T_B value did not reach beyond 5-8 K despite having a very large U_{eff} value.¹³⁻³⁴ The breakthrough in lanthanide-based SIM was achieved in 2016 when a pseudo pentagonal bipyramidal $[\text{L}_2\text{Dy}(\text{H}_2\text{O})_5][\text{I}]_3 \cdot \text{L}_2 \cdot \text{H}_2\text{O}$ (**1**, $\text{L} = {}^t\text{BuPO}(\text{NH}^i\text{Pr})_2$) molecule was reported with a T_B value of 12 K (based on ZFC/FC) by some of us,³⁵ and at the same time several pseudo D_{5h} point group molecules were also reported by others with slightly smaller T_B values.³⁵⁻³⁸ We have further demonstrated the role of weak equatorial and strong axial ligand fields in designing high-performance SIM with very large U_{eff} and T_B values. This is followed by several pseudo pentagonal bipyramidal complexes in the literature where U_{eff} and T_B values reached as high as 1800 K and 36 K, respectively.^{36-37, 39-45} Later years witness tremendous increase in T_B values by a class SIMs commonly called Dysprosocenium class of molecules taking the T_B values as high as 80 K – albeit these class of molecules lack ambient stability pitching further challenges in taking these molecules to end-user applications.⁴⁶⁻⁴⁹

The magnetization relaxation of a SIM occurs via quantum tunnelling of magnetization (QTM) at very low temperatures due to the low symmetry component of the crystal field (CF).¹² At higher temperatures, it occurs through various spin-vibrational coupling like direct, Raman and Orbach pathways.¹² The direct process is a barrierless process which involves a direct transition between the "up" to "down" spin state, where the crystal lattice absorbs the energy released by the spin system.¹² The Orbach process is a multiple one-phonon phenomenon where magnetization relaxation occurs by a sequential absorption of phonons involving excited m_J states and then sequential emission of phonons to reach the ground state by reversing its magnetization.^{1-5, 50-52} This Orbach relaxation becomes very slow at low temperatures due to the lack of thermally available phonons to initiate this process.^{1-2, 4-5, 53} The Raman process is similar to Orbach, but it involves a virtual intermediate state of lattice and spin system which destroys the blocking barrier of magnetization reversal.

The three key features that are commonly employed to block the magnetization relaxation of an SMM are (i) a large m_J ground state ($m_J = \pm J$), (ii) designing a ligand environment around the metal centre to maintain a large separation between successive m_J levels of the bistable ground state (iii) a minimal admixing between the m_J states.^{1-4, 54} It is worthwhile to mention that the search for potential SIMs fulfilling the criterion (i), (ii), and (iii) is considered within the framework of the Orbach process. In this regard, the recent discovery of dysprosocenium SIMs has divulged the importance of spin-vibration coupling in controlling magnetization

relaxation.^{5, 46, 48-49} Although synthetic chemists extensively tried to control spin-vibration coupling through molecular design, design principles to control such effects are still elusive.⁴⁹ Therefore, to design high-performant SIMs, one needs to deepen the understanding of spin-vibrational coupling by theoretical methods.

A recent theoretical study also demonstrated that further enhancement of T_B and U_{eff} is challenging in dysprosium complexes as magnetic anisotropy reaches its axial limit.⁵ In this regard, the pseudo D_{5h} family of SIMs have an edge due to a large variation in the U_{eff} (37-1200 cm^{-1}) and T_B (2-30K) values observed, offering significant room for further improvement in T_B values.^{10-11, 35-40, 42, 55-67} It is noteworthy to mention that raising the T_B value from 60 K to 80 K in dysprosocenium complexes is related to the judicious design of ligands to efficiently decouple the vibrationally active normal mode coupled to the spin states.^{46, 48} To fine-tune the magnetic anisotropy in pentagonal bipyramidal Dy(III) SIMs, one needs a thorough understanding of the related spin-phonon coupling. The spin-vibration coupling occurs when a molecular vibration (due to the temperature) modulates the crystal field Hamiltonian of a metal centre. This coupling is directly related to spin-lattice relaxation, and over the past few years, an in-depth investigation of spin-vibration coupling by *ab initio* CASSCF methods has been reported. However, such studies are limited only to a handful of molecules as these calculations are computationally demanding and alternative methods which are still accurate in understanding the spin-phonon/vibrational problem are of supreme interest in the community.^{1-5, 38, 46, 67} Although efforts have been made to employ semiempirical methods, they lack the predictive potential for such systems.⁸⁻⁹

In this work, employing a combination of DFT and *ab initio* SA-CASSCF/RASSI-SO/SINGLE_ANISO approach, we have studied in detail the pseudo D_{5h} family of molecules to thoroughly understand their electronic structure and spin-vibrational correlations to the blocking temperatures. The method developed here relies on chemical intuition and undercuts the need to perform hundreds of CASSCF calculations to extract the relevant chemical insights. For our study, we have chosen five pseudo pentagonal bipyramidal Dy(III) SIMs, namely [Dy(bbpen)Br] (**1**, $\text{H}_2\text{bbpen}=\text{N},\text{N}'\text{-bis}(2\text{-hydroxybenzyl})\text{-N},\text{N}'\text{-bis}(2\text{-methylpyridyl})\text{ethylenediamine}$),³⁸ [Dy(OCMe₃)Br(THF)₅][BPh₄] (**2**)⁴³ and [Dy(OSiMe₃)Br(THF)₅][BPh₄] (**3**)⁴³, [Dy(L^{N5})(Ph₃SiO)₂](BPh₄).CH₂Cl₂ (**4**)⁶⁸ and [L₂Dy(H₂O)₅][I]₃.L₂.H₂O (**5**, L = ^tBuPO(NHⁱPr)₂)³⁵ where the U_{eff} and T_B (from FC/ZFC) range from 400-1200 cm^{-1} and 5-12 K, respectively. For the dysprosocenium class of molecules, T_B values are approximately in the range of ~3-5% of the reported U_{eff} values, but in complexes, **1-5** T_B is much smaller (~1-3 % of the U_{eff}), suggesting a room for further enhancement. Here by performing the spin-vibration calculations, we aim to address the followings (i) Why do the pseudo D_{5h} Dy(III) SIMs, despite possessing similar structures and U_{eff} values, have a diverse set of T_B values (4.5 K - 36 K)? (ii) What is the nature of vibrationally active normal mode causing the transition from ground KD to first excited KD in this class of compounds? (iii) how these spin-phonon vibrations are correlated to the T_B values? (iv) Is it possible to quench vibrations that cause relaxation via judicious choice of ligand design? (v) What are the design clues that needs to be factored to enhance the T_B values in this class of molecule?

3. Results and Discussion

3.1. Controlling U_{eff} and T_{B} in complex **1** by intuitive chemical substitution using Spin-Phonon Lens

Complex **1** (see Figure 1a) is reported to exhibit zero-field slow relaxation of magnetization with an U_{eff} and T_{B} value of 712 cm^{-1} and 14 K (sweep rate 20 Oe/s), respectively.³⁸ Earlier *ab initio* calculations on this complex revealed magnetization relaxation via the third excited KD, yielding an U_{cal} value of 721 cm^{-1} , which agrees well with the U_{eff} value. Furthermore, the ground and first excited state of this complex possess a dominant contribution $m_{\text{J}} = |\pm 15/2\rangle$ and $|\pm 13/2\rangle$ respectively that fits perfectly to the criteria that we have set forth (see computational methodology). The geometry optimization of **1** yields a geometry closely resembling the X-ray structure (Table S1, Figure S1 and Appendix S1). This is also reflected in the *ab initio* CASSCF calculations, where both X-ray and optimized geometries yield a similar energy spectrum, g-tensors and CF parameters (Table S2-S3), affirming faith in the methodology used in obtaining good geometries for estimating magnetic properties.

For the spin-phonon coupling calculations, ten vibrational modes at 123.7 (ω_1), 142.1 (ω_2), 184.5 (ω_3), 192.8 (ω_4), 210.7 (ω_5), 214.4 (ω_6), 242.1 (ω_7), 289.1 (ω_8), 309.6 (ω_9) and 358.9 (ω_{10}) cm^{-1} were chosen as per the criteria described in the methodology section (see Figure 1 and S1-S2). The coupling constant C_k of ten high-intensity vibrational modes of **1** are depicted in Figure 1 (see Tables S5-S7 and Figures S3-S12). Figure 1 implies that the ω_4 and ω_5 vibrational modes are associated with a large coupling constant and, therefore, should cause the $|\frac{15}{2}, \pm \frac{15}{2}\rangle \rightarrow |\frac{15}{2}, \pm \frac{13}{2}\rangle$ transition for magnetization relaxation. To attain the CF parameter modulation of each mode, one needs to include its thermal population via Boson number (B_k) along with coupling strength (Figure 1). For complex **1**, the B_k values are negligible below 14 K , and this temperature coincides with the reported T_{B} value. At higher temperatures, each mode gains momentum and exhibits larger variations in the CF parameter with a slope $\frac{k_{\text{B}}}{\omega_k}$. Among several vibrations, the ω_4 mode yields the most significant contribution in the entire temperature range, - thanks to its larger coupling strength and moderate frequency value. Further analysis suggests that these modes are associated with a large oscillator strength and are in the range of the KD1-KD2 energy gap, though the absolute magnitude is smaller, as witnessed in earlier cases.^{46, 48} The ω_4 vibrational mode of **1**, which is suggestive of being responsible for magnetization relaxation, has several functional group movements (Figure 1 and S2). The significant vibrational movement was noted for (i) the hydrogen atom at the meta position of the pyridine rings, (ii) the para position of the phenolate rings, and (iii) the $-\text{CH}_2$ linker groups attached to pyridine and phenolate donors atoms (Figure 1 and Figure S2). As these were the key vibrations correlated with magnetization relaxation, any attempt to quench these vibrations is expected to enhance the effective energy barrier/ T_{B} values. The substitution of these hydrogens with heavier atoms is therefore expected to improve the performance.

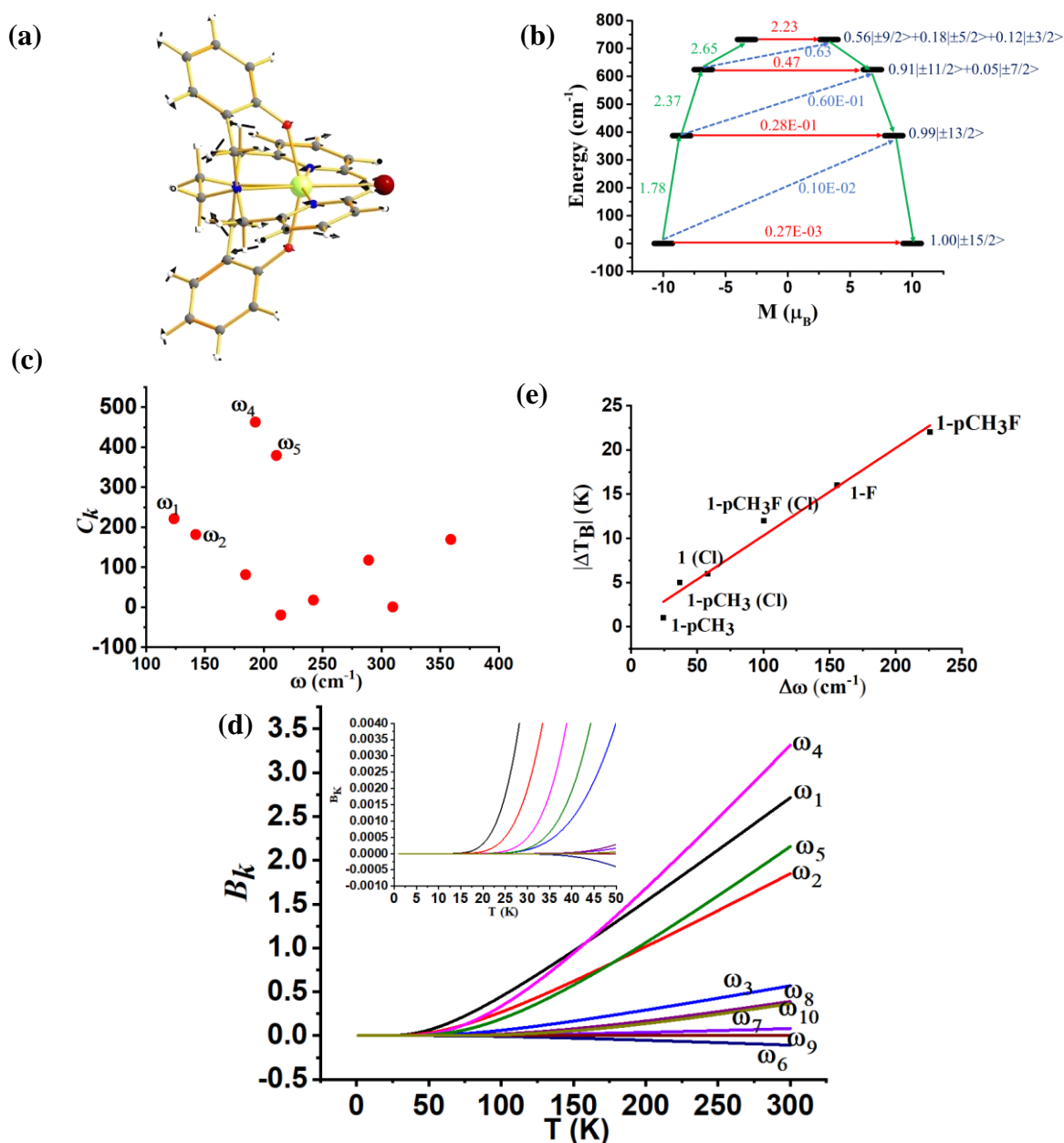


Figure 1. (a) The molecular vibration of **1** corresponds to the ω_4 frequency (cm^{-1}). Here the arrows represent the scaled vector of displacement. Colour code: Dy-yellow, Br-brown, O-red, N-blue, C-grey and H-white. (b) The mechanism of magnetization relaxation of optimized geometry of **1**. Here red arrows denote the QTM for the ground state and TA-QTM for the excited state. The blue arrows signify the Orbach process. The green arrow implies the most probable pathway for magnetization relaxation. The blue character denotes the m_J composition of KDs. (c) The spin-vibrational coupling C_k for the ten high-intensity vibrational modes of **1**. (d) A comparison of the change in T_B values with the change in ω_4 normal mode of **1**. A good linear fit (slope = 0.099 and intercept = 0.416) is obtained with $R^2 = 0.97$. (e) The B_k CF parameter thermal modulation for the ten high-intensity vibrational modes of **1** (see inset for the temperature at which deviation occurs for each vibrational mode).

A quick Cambridge structural database search for such substituted geometries reveals substitution of the meta position hydrogen atom by fluorides reported by Li and co-workers [(Dy(bbpen-F)Br], see Figure 2).³⁹ We then performed *ab initio* calculations on the optimized geometry (called **1-F**, Appendix S2) that yields the U_{cal} value of 763.2 cm^{-1} , which is ca. 50 cm^{-1} higher, suggesting enhancement in effective energy barrier via this substitution as

expected (Table S8). This value matches with the experimentally reported U_{eff} value of 798.4 cm^{-1} . More importantly, as expected, the pyridinic contribution to the ω_4 frequencies diminished, leading to blue shift (192.8 (**1**) cm^{-1} \rightarrow 348.4 cm^{-1} (**1-F**), Table S9) of these frequencies in **1-F**, and these are accompanied by a substantial enhancement in the T_B values (14 K @20 Oe/s to 30K@20 Oe/s). A similar CCDC search also yielded another structure where the para position of the phenolate hydrogen was substituted by CH_3 groups ([Dy(bbpen- CH_3)Br], **1-pCH₃**, see Figure 3). The *ab initio* calculations on the optimized geometry of **1-pCH₃** (Appendix S3) yield the U_{cal} value of 764.1 cm^{-1} (Table S10), reaffirming a larger value compared to **1**. Not only this value matches the experimentally reported value of 806.9 cm^{-1} , but the T_B values are also marginally larger (15 K@20Oe/s). Furthermore, as expected, the phenolate contribution to the ω_4 frequencies diminished, leading to a blue shift (192.8 (**1**) cm^{-1} \rightarrow 217.2 (**1-pCH₃**) cm^{-1} , Table S11) of these frequencies in **1-pCH₃**. Furthermore, an enhancement of the computed B_2^0 axial CF parameter is observed in **1-F** and **1-pCH₃** compared to **1** (Table S3).

A further search yielded another structure where the para position of the phenolate hydrogen was substituted by CH_3 groups and para position hydrogen atoms by fluorides ([Dy(bmbpen-F)Br], **1-pCH₃F**, see Figure 2).⁶⁹ The *ab initio* calculations on the optimized geometry of **1-pCH₃F** (Appendix S4) yielded the U_{cal} value of 842.5 cm^{-1} , reaffirming a larger value compared to **1**, **1-F** and **1-pCH₃** (Table S12). Although the U_{cal} value is slightly overestimated compared to the U_{eff} value of 782.3 cm^{-1} , more importantly, the T_B value (36 K@20Oe/s) is significantly higher than all **1**, **1-F** and **1-pCH₃**. As expected, the phenolate and pyridine contribution to the ω_4 frequencies diminished, leading to a blue shift (192.8 (**1**) cm^{-1} \rightarrow 418.6 (**1-pCH₃F**) cm^{-1} , Table S13) of these frequencies in **1-pCH₃F**. This reiterates that the approach developed here not only hints at ligand design that targets enhancement in U_{eff} values but also the vibrations that are strongly correlated to the T_B values.

Furthermore, the $-\text{CH}_2$ linker groups attached to pyridine and phenolate donors were found to have a significant vibrational movement. We attempted to alter those C–H bonds and modelled the corresponding $-\text{CH}_2$ groups by $-\text{C}(\text{Me})_2$ groups (see Figure 2 model **1-CH₃**). For this model, the O–Dy–O angle increases to 162.9° and the Dy–N bond length elongates to 2.948 Å (Table S1, Figure 2 and Appendix S4). The *ab initio* CASSCF calculations on **1-CH₃** reveal an increase in the KD1-KD2 energy gap, energy splitting of the eight KDs and axial B_2^0 CF parameter compared to **1** by 0.14, 0.50 and 0.06 %, respectively (Table S3 and S14). The magnetization relaxation in **1-CH₃** was found to occur via the third excited KD, resulting in the U_{cal} value of 1039.5 cm^{-1} , which is ca. 300 cm^{-1} larger than **1**. Quite interestingly, a blue shift of vibrational mode is observed from **1** to **1-CH₃** (192.8 (**1**) cm^{-1} \rightarrow 480.6 (**1-CH₃**) cm^{-1} , Table S15). The blocking barrier and normal models of **1**, **1-F**, **1-pCH₃**, **1-pCH₃F** and **1-CH₃** imply that there is a strong correlation with the ω_4 normal mode with the T_B values. Therefore, we have made a linear regression with the change in the ω_4 normal mode with the change T_B values for all the above complexes along with three additional complexes with a similar structural framework (vibrational modes for 134.9 cm^{-1} for [Dy(bbpen)Cl] (**1 (Cl)**), 229.7 cm^{-1} for Dy(bbpen- CH_3)Cl] (**1-pCH₃ (Cl)**) and 293.3 cm^{-1} for [(Dy(bbpen-F)Cl] (**1-F (Cl)**), see Tables S16-S17 of the ESI). A linear relationship offers an excellent fit between these two parameters with an R^2 value of 0.97 (see Figure 1). A simple extrapolation based on this correlation suggests the largest possible T_B value of ~42.9 K for **1-CH₃** if made.

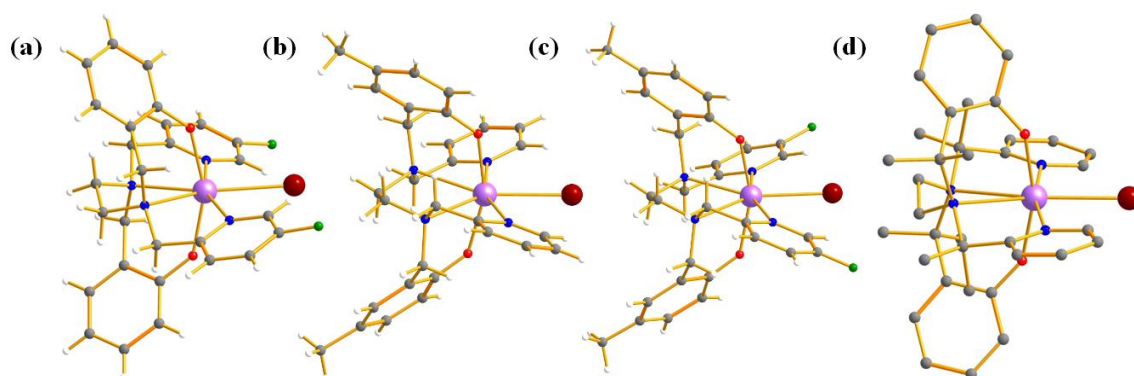


Figure 2. The crystal structure of (a) **1-F** (b) **1-pCH₃** (c) **1-pCH₃F**. (d) The optimized geometry of **1-CH₃**. Here, the hydrogens are omitted for clarity. Colour code: Dy-blue violet, Br-brown, F-green, O-red, N-blue, C-grey.

3.2. Role of Equatorial ligand field in dictating U_{eff} and T_{B} in Complexes **2** and **3**

The magnetic properties of complexes **2** and **3** (Figures 3 and 4) were studied by Zheng and co-workers along with a family of other pseudo D_{5h} SMMs. Both of them show zero-field slow relaxation of magnetization with U_{eff} values of 569 ± 126 (**2**) and 509 ± 49 cm^{-1} (**3**), respectively, with a T_{H} (blocking temperature derived from hysteresis loop, see for example [43]) value of 9 K (sweep rate 15 Oe/s).⁴³ These two complexes are structurally similar, except that the -OCMe₃ group present in **2** is replaced by the -OSiMe₃ group in **3** (Figures 3 and 4).⁴³ This replacement leads to a 0.07 Å enhancement in the Dy-OSiMe₃ bond length in **3** compared to Dy-OCMe₃ bond length in **2**, resulting in a lower U_{eff} in **3** compared to **2** (Tables S20-S21). The geometry optimization of **2** and **3** also yield geometries and magnetic properties similar to that of X-ray structures (Tables S20-S21, Figures S13-S14 and Appendix S5-S6), particularly the estimated CF parameters are strikingly similar (see Table S22).

To find out the most important vibrational modes for spin-phonon coupling, we have selected ten vibrational modes with the energy of 143.5 (ω_1), 188.5 (ω_2), 221.8 (ω_3), 226.9 (ω_4), 229.4 (ω_5), 235.8 (ω_6), 243.6 (ω_7), 279.6 (ω_8), 289.6 (ω_9) and 300.7 (ω_{10}) cm^{-1} (Figures 3 and S15) for **2** and ten vibrational modes with the energy of 173.6 (ω_1), 199.9 (ω_2), 201.4 (ω_3), 210.9 (ω_4), 211.4 (ω_5), 217.6 (ω_6), 229.7 (ω_7), 308.2 (ω_8), 311.3 (ω_9), 359.4 (ω_{10}) cm^{-1} for **3** (Figures 4, S16 and Tables S23-S24). By analyzing the coupling strength and thermal dependence of $B_2^{\pm 1}$ CF parameter (Figures 3-4, Figures S17-S36, and Tables S25-S30), we found that ω_3 vibrational mode for **2** and ω_5 vibrational mode for **3** is responsible for the spin-phonon coupling from KD1 to KD2 transition. These vibrational modes have a significant force on many functional groups. Among these vibrations, the displacement of Dy ion was found to be prominent (Figures 3-4). As these vibrations are responsible for magnetization relaxation, any attempt to quench these vibrations will increase the $U_{\text{eff}}/T_{\text{B}}$ values. Therefore, to quench the in-plane movement of the Dy atom, there are two approaches (i) substitute the Dy with a heavier isotopic analogue⁷⁰⁻⁷², (ii) enhance the Dy-ligand equatorial bond strength. To achieve this, we have replaced the five THF molecules in the equatorial plane in complexes **2** and **3**

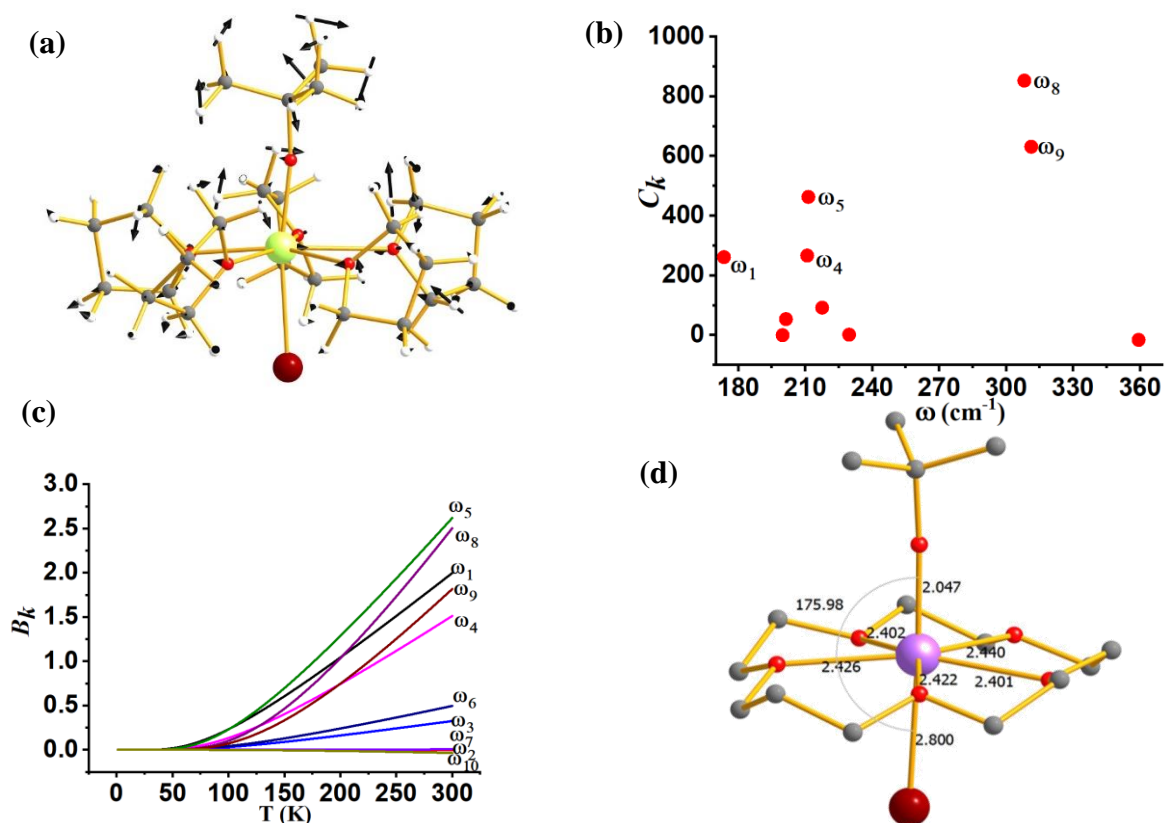


Figure 3. (a) The molecular vibration of **2** corresponds to the $\omega_3 \text{ cm}^{-1}$. Here the arrows represent the scaled vector of displacement. Colour code: Dy-yellow, Br-brown, Si-purple, O-red, C-grey and H-white. (b) The spin-vibrational coupling C_k for the ten high intensity vibrational modes of **2**. (c) The B_k parameter thermal modulation for the ten high intensity vibrational modes of **2** (see inset for the temperature at which deviation occurs for each vibrational mode). (d) B3LYP optimized models structures of **2-crown**, with important structural parameters (bond lengths are shown in Å and bond angles are shown in °).

with a 16-crown-5 macrocyclic ring (models **2-crown** and **3-crown**, see Figures 5). Although these are models at present, some of us have recently reported [$\{(18\text{-crown-6})\text{Ln}(\text{dippH})_3\}\{\{(18\text{-crown-6})\text{Ln}(\text{dippH})_2(\text{dippH}_2)\}\} \cdot [\text{I}_3]$ (with Ln = Ce, Pr and Nd and $\text{dippH}_2 = 2,6\text{-diisopropylphenylphosphates}$) complexes of a similar kind with various lanthanide ions exhibiting attractive SIM characteristics.⁷³⁻⁷⁵ The **2-crown** and **3-crown** have shorter Dy-O bond lengths (reduced by $\sim 0.02\text{-}0.04 \text{ \AA}$, except Dy-Br bond length) and a marginal $1\text{-}2^\circ$ increase in O-Dy-Br angle compared to **2** and **3** (Figure 4(d) and Figure 5(d), Tables S18-S19 and Appendix S7-S8).

The *ab initio* calculations reveal enhancement of the KD1-KD2 energy gap, the energy splitting of eight KDs as well as axial B_2^0 CF parameters in **2-crown** (**3-crown**) compared to **2** (**3**) (Tables S22, S31-S32). The magnetization relaxation of **2-crown** (**3-crown**) is expected to take place via 3rd excited KD due to the large TA-QTM value, yielding an U_{cal} value of 832.8 cm^{-1} (869.1 cm^{-1} , ca. 300 (350) cm^{-1} larger than **2** (**3**). It is worthwhile to mention that the contribution of the in-plane movement of the Dy atom to the ω_3 (ω_5 for **3-crown**) frequencies diminished, leading to blue shift (221.8 (**2**) $\text{cm}^{-1} \rightarrow 373.7$ (**2-crown**) cm^{-1} and 211.4 (**3**) $\rightarrow 373.8 \text{ cm}^{-1}$ (**3-crown**), Tables S33-S34) of these frequencies and this is expected to enhance the T_B

values. A simple extrapolation based on the earlier correlation of **1** suggests the largest possible T_B value of ~ 24.4 K and 25.5 K for **2-crown** and **3-crown**, respectively.

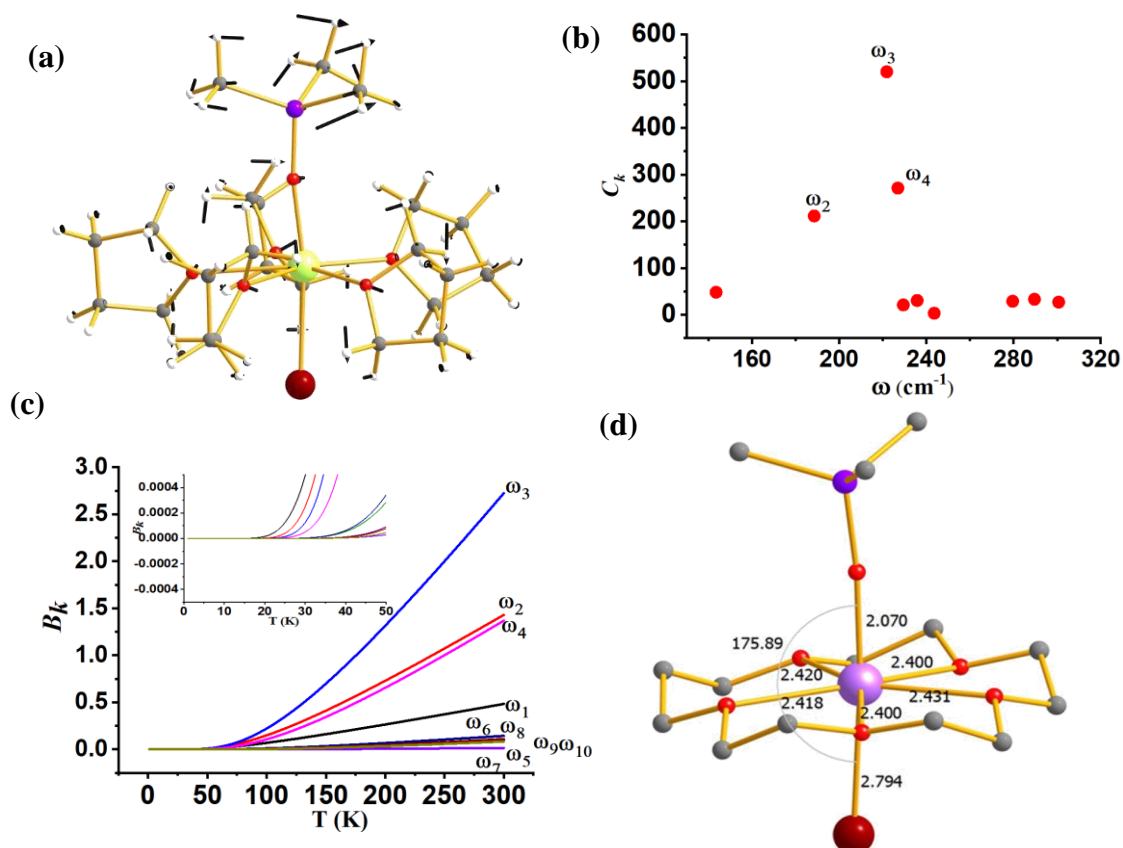


Figure 4. (a) The molecular vibration of **3** corresponds to the ω_5 cm^{-1} . Here the arrows represent the scaled vector of displacement. Colour code: Dy-yellow, Br-brown, Si-purple, O-red, C-grey and H-white. (b) The spin-vibrational coupling C_k for the ten high intensity vibrational modes of **3**. (c) The B_k CF parameter thermal modulation for the ten high intensity vibrational modes of **3** (see inset for the temperature at which deviation occurs for each vibrational mode). (d) B3LYP optimized models structures of **3-crown** with important structural parameters (bond lengths are shown in Å and bond angles are shown in $^\circ$).

3.3. Role of N–H Vibrations in Fine-Tuning the U_{eff} and T_B values in Complex **4**

In the earlier section, we have shown how a crown-ether ligand in the equatorial position quenches the low-energy vibrational modes that are correlated with the magnetization relaxation. These two models are predictions, but an analogous complex containing a macrocyclic Schiff-based ligand at the equatorial position has been reported earlier by Murrie and our group $[\text{Dy}(\text{L}^{\text{N}5})(\text{Ph}_3\text{SiO})_2](\text{BPh}_4)\cdot\text{CH}_2\text{Cl}_2$ (**4**, Figure 5).⁶⁸ However, due to the complexity of the functional groups involved in the equatorial position, similar vibrations in **4** were absent. We have carefully analyzed various vibrational modes at the equatorial plane, which could help improvise performance of **4**. Complex **4** exhibits zero-field slow relaxation of magnetization with a very large U_{eff} of 791.4 cm^{-1} and T_B of 14 K (sweep rate 100 Oe/s). The *ab initio* calculations on this complex yield a U_{cal} value that is in excellent agreement with the U_{eff} value reported (791.4 vs 722.8 cm^{-1}). On the other hand, the O–Dy–O angle reduces to 2.5° in the optimized structure compared to the X-ray geometry (Table S35 and Figure S37),

and the optimized geometry yields magnetic characteristics and CF parameters which are similar to the X-ray structure (see Table S36-S37).

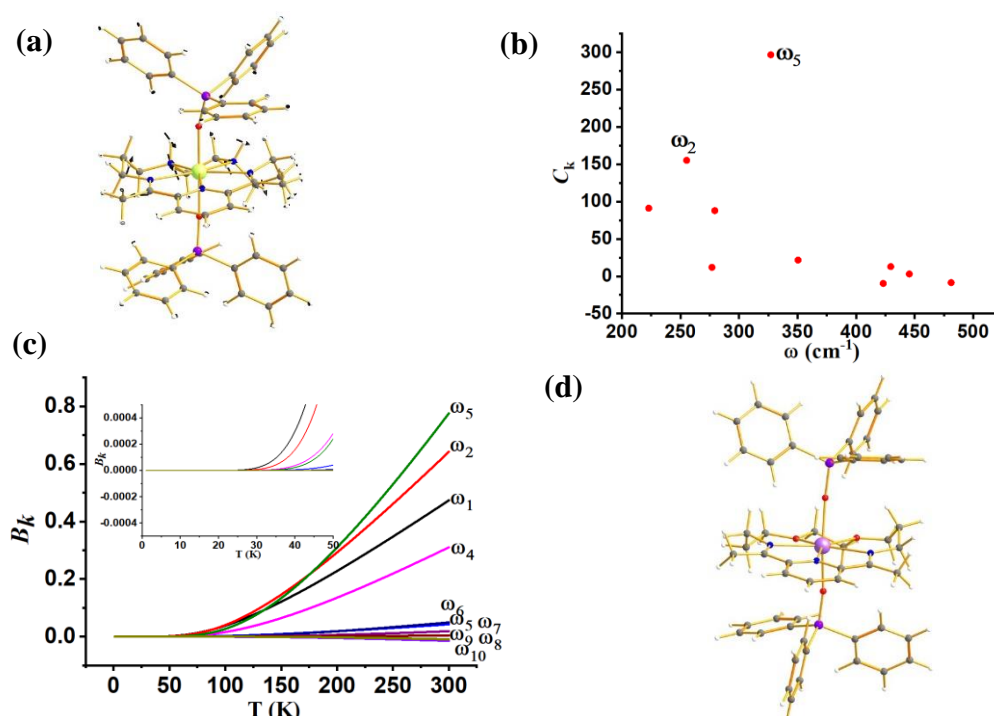


Figure 5. (a) The molecular vibration of **4** corresponding to the ω_3 vibrational mode. Here the arrows represent the scaled vector of displacement. Colour code: Dy-yellow, Si-purple, O-red, N-blue, C-grey and H-white. (b) The computed IR spectrum of **4** in the range of KD1-KD2 energy gap. The arrows denotes the vibrational modes that have been taken into consideration in our study. (c) The spin-vibrational coupling C_k for the ten high intensity vibrational modes of **4**. (d) The B_k CF parameter thermal modulation for the ten high intensity vibrational modes of **4** (see inset for the temperature at which deviation occurs for each vibrational mode). (e) The optimized geometry of **4-N3O2**.

For the spin-phonon coupling calculations of **4**, we selected ten vibrational modes at 222.9 (ω_1), 255.3 (ω_2), 276.9 (ω_3), 279.3 (ω_4), 327.1 (ω_5), 350.4 (ω_6), 423.1 (ω_7), 429.5 (ω_8), 445.4 (ω_9), and 481.1 (ω_{10}) cm^{-1} (Figure S38 and S89) with a large oscillator strength in the range of KD1-KD2 energy gap. By analyzing the coupling strength and thermal dependence of $B_2^{\pm 1}$ CF parameter (Figure 5, S39-S48 and Table S39-S41), we found that the ω_5 vibrational mode is likely to be responsible for the spin-phonon coupling of KD1→KD2 transition, and this vibration is found to be correlated to the N–H vibrations present in the equatorial plane (Figure 5). To quench these vibrations, we have replaced the -NH group with its isoelectronic analogue oxygens resulting in **4-N3O2** (Figure 5 and Appendix S10). As expected, a blue shift of the ω_3 vibrational mode (327.1 (**4**) cm^{-1} → 377.2 cm^{-1} (**4-N3O2**) cm^{-1} , Table S43) is observed in **4-N3O2**. The *ab initio* calculations on **4-N3O2** revealed an enhancement in the energy splitting of the eight KDs compared to **4** (Table S42). The magnetization relaxation of **4-N3O2** occurs via third excited KD due to significant transverse anisotropy yielding an U_{cal} value of 998.7 cm^{-1} (Table S42), which is ca. 200 cm^{-1} larger than **4**. A simple extrapolation based on an earlier correlation of **1** suggests the largest possible T_B value of ~19.4 K for **4-N3O2** if made.

3.4. Role of out-of-plane bending of water in Controlling the U_{eff} and T_{B} values in Complex **5**

In this last section, we will unveil the nature of vibration correlated with the magnetization relaxation in $[\text{L}_2\text{Dy}(\text{H}_2\text{O})_5]^{3+}$ family of SMMs where a large U_{eff} and T_{B} were observed (Figure 6).^{35-36, 56-57, 63, 76} The complex **5** is reported to possess a large U_{eff} value and T_{B} value of 453 cm^{-1} and 12 K, respectively.³⁵ The *ab initio* CASSCF calculations on the X-ray structure of **5** indicated that the stabilization of $m_{\text{J}} = |\pm 15/2\rangle$ and $|\pm 13/2\rangle$ in the ground and first excited state, respectively. The magnetization relaxation occurs via the second excited KD, yielding a U_{cal} value of 471.3 cm^{-1} , slightly overestimated compared to the U_{eff} value (Table S44). The *ab initio* calculations on this optimized structure reveal a moderate change in energy values and g tensors compared to the X-ray geometry as the equatorial oxygens become out-of-plane in the optimized structure (Table S45, Figure S49 and Appendix S11). However, the computed CF parameters in the optimized structure are similar (Table S44, S46) to the X-ray structure, and more importantly, the ground and first excited KD possess dominant contributions from $m_{\text{J}} = |\pm 15/2\rangle$ and $|\pm 13/2\rangle$ state, respectively.

For the spin-phonon coupling calculations on **5**, we selected twenty-nine vibrational modes (shown in Figures 7, S50-S59 and Table S47-S50). The CF parameter values at the several displacements of these normal modes are shown in Figure S60-S88. By analyzing the coupling strength and thermal dependence of $B_2^{\pm 1}$ CF parameter, we find that the ω_1 (98.7 cm^{-1}), ω_4 (121.7 cm^{-1}) and ω_{13} (174.2 cm^{-1}) vibrational modes are likely responsible for the spin-phonon coupling of KD1 \rightarrow KD2 transition. These ω_1 and ω_4 and ω_{13} vibrational modes have a significant movement for the equatorial oxygens (out-of-plane) and axial $-\text{CH}_3$ groups. Therefore, quenching the movement of the equatorial oxygens should increase the U_{eff} and T_{B} values of **5**. In this regard, a CCDC search yielded $[\text{Dy}(\text{dppbO}_2)1.5(\text{H}_2\text{O})_5]\text{I}_3 \cdot (\text{dppbO}_2) \cdot \text{H}_2\text{O} \cdot \text{EtOH}$ (**5a**, dppbO₂ = 1,4-butylenebis(diphenylphosphine oxide)) and $\{[\text{Dy}(\text{dppbO}_2)(\text{H}_2\text{O})_5]\text{I}_3 \cdot 2(\text{Ph}_3\text{PO}) \cdot 0.5\text{H}_2\text{O} \cdot 0.5\text{EtOH}\}_n$ (**5b**) studied by Tong and co-workers.⁷⁷ Quite interestingly, moving from dinuclear (**5a**) to the 1D polymer (**5b**) leads to improving the equatorial planarity of the water molecules. As a result of this, an almost two times increase in the T_{B} value is observed from **5a** to **5b** (FC/ZFC T_{B} value is 4.5 K (9.3 K) for **5a(5b)**), supporting our theoretical predictions.

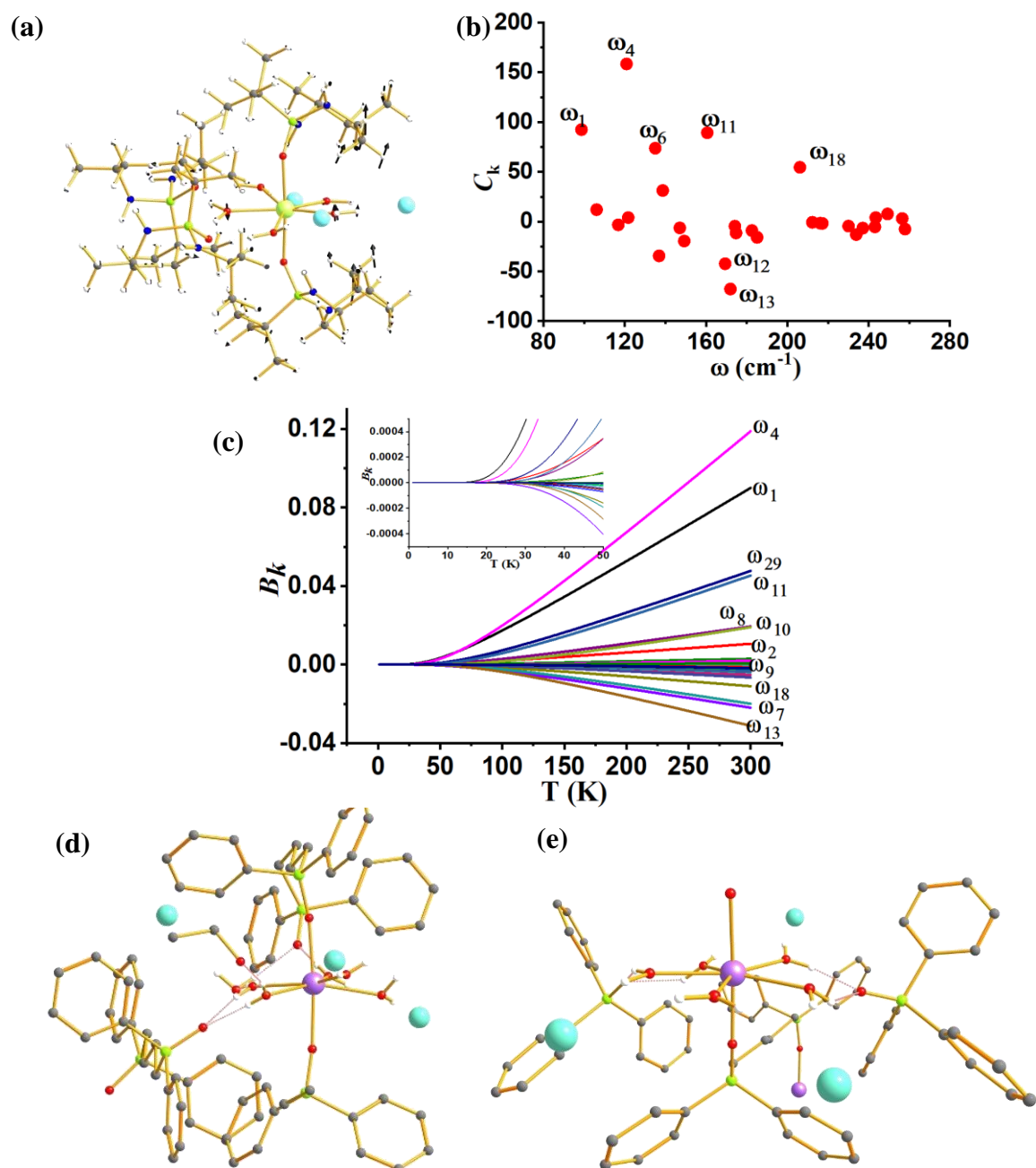


Figure 6. (a) The molecular vibration of **5** corresponds to the ω_1 vibrational mode. Here the arrows represent the scaled vector of displacement. (b) The computed IR spectrum of **5** within the KD1-KD2 energy gap. The arrows denotes the vibrational modes that have been taken into consideration in our study. (c) The spin-vibrational coupling C_k for the twenty nine high intensity vibrational modes of **5**. (d) The B_k CF parameter thermal modulation for the twenty nine high intensity vibrational modes of **5** (see inset for the temperature at which deviation occurs for each vibrational mode). (e) The X-ray structure of complex **5a** (only monomer is shown here). (f) The X-ray structure of complex **5b**. In case of complexes **5a** and **5b**, the hydrogens except connected to water are removed for clarity. Colour code: Y-yellow, Dy-blue violet, I-aqua, P-green, O-red, C-grey and H-white.

4. Discussion

The advancement in molecular nanomagnets has led to the growth of plenty of SMMs with very large U_{eff} values, but the T_B values remain a small fraction of it due to the under-barrier

relaxation processes. In this regard, the study of spin-phonon coupling in dysprosocenium complex $[\text{Dy}(\text{Cp}^{\text{ttt}})_2][\text{B}(\text{C}_6\text{F}_5)_4]$ ($\text{Cp}^{\text{ttt}} = \{\text{C}_5\text{H}_2^t\text{Bu}_{3-1,2,4}\}$) has made an important breakthrough, not only because this holds record high T_B value, but also they have shown which vibrations are linked with the magnetization relaxation.⁴⁶ Based on their study, two years later, another novel dysprosocenium SIM, $[(\text{Cp}^{\text{iPr5}})\text{Dy}(\text{Cp}^*)]^+$ (Cp^{iPr5} , penta-isopropylcyclopentadienyl; Cp^* , pentamethylcyclopentadienyl) was discovered quenching the vibrations governing the magnetization relaxation.⁴⁸ On the other hand, Lunghi and co-workers have recently demonstrated the role of anharmonic phonons in dictating the under-barrier magnetization relaxation.^{1-4, 51, 54, 78-80} Therefore, spin-phonon coupling calculations are of utmost importance to unveil the underlying physical process of magnetization relaxation and provide a clear indication of how the relaxation process is linked with molecular motions. As a result, it can give the design criteria of potential SMM with chemical tuning to quench the vibrations associated with Orbach and Raman relaxation process.

The calculations of spin-phonon coupling require thousands of *ab initio* calculations which are computationally demanding and often do not directly yield chemical insights to improve the T_B values. Furthermore, we have confined ourselves to the vibrations having significant oscillator strength that also lies within the KD1-KD2 energy gap so that magnetization relaxation from $m_J = |\pm 15/2\rangle$ to $|\pm 13/2\rangle$ of ground ${}^6\text{H}_{15/2}$ state can be gauged. Within this approximation, we have performed spin-phonon coupling calculations on complexes **1-5**. It should be noted that the ground and first excited KD are not always possessed dominant contributions from $m_J = \sim \pm 15/2\rangle$ and $\sim \pm 13/2\rangle$ states, respectively, in most of the Dy(III) SIMs. For complexes with the different ground and first excited states, one has to follow a "knockout" procedure developed by Chilton and co-workers to determine the vibrational mode linked with the magnetization relaxation.⁵ The Escalera-Arino method, on the other hand, proposed computation of the spin-phonon term for each vibrational mode (C_k ; see methodology section for details) and thermal population in the vibrational modes were accounted via the Bose-Einstein statistic term (B_k).⁹³⁻⁹⁴ In this work, we have adopted this method to compute the spin-phonon coupling on selected vibrational levels. Our calculations reveal that not only the atoms in the first coordination sphere but also those in the secondary coordination sphere affect the magnetization relaxation. In the case of complex **5**, the out-of-plane bending vibrations of the equatorial oxygens govern the magnetization relaxation, and therefore disrupting this movement might increase the U_{eff} and T_B values. It is worth mentioning that in the Cl and Br analogue of complex **5** ($[\text{L}_2\text{Dy}(\text{H}_2\text{O})_5][\text{Cl}]_3 \cdot \text{L}_2$ (**6**) and $[\text{L}_2\text{Dy}(\text{H}_2\text{O})_5][\text{Br}]_3 \cdot \text{L}_2 \cdot \text{H}_2\text{O}$ (**7**), $\text{L} = {}^t\text{BuPO}(\text{NH}^i\text{Pr})_2$), the U_{eff} and T_B values decrease from I to Br and Cl analogue (T_B (FC/ZFC) = 12.9 K for I, 11.6 K for Br and 8.2 K for Cl).⁸¹ This may be ascribed to the equatorial planarity of water molecules, which increases from I to Br to Cl analogues of **5**. The vibrational modes should be near-resonant with the KD1-KD2 energy gap for the magnetization relaxation in the Orbach regime. In our case, the energy of the vibrational modes is far lower than the KD1-KD2 energy gap, diminishing the T_B values. From the literature, we have also found that an increase in the T_B value from $[\text{Dy}(\text{OPCy}_3)(\text{H}_2\text{O})_5]\text{Cl}_3 \cdot \text{OPCy}_3 \cdot \text{H}_2\text{O} \cdot \text{EtOH}$ (**8**, T_B (FC/ZFC) = 8K) to $[\text{Dy}(\text{OPCy}_3)(\text{H}_2\text{O})_5]\text{Br}_3 \cdot 2\text{OPCy}_3 \cdot 2\text{H}_2\text{O} \cdot 2\text{EtOH}$ (**9**, T_B (FC/ZFC) = 11K).³⁶ On the other hand, a significant improvement in the blocking barrier is observed going from $[\text{Dy}(\text{HMPA})_2(\text{H}_2\text{O})_5]\text{Cl}_3 \cdot \text{HMPA}$ (**10**, $U_{\text{eff}} = 460$ K) to $[\text{Dy}(\text{HMPA})_2(\text{H}_2\text{O})_5]\text{I}_3 \cdot 2\text{HMPA}$ (**11**, $U_{\text{eff}} = 600$ K).⁵⁷ The U_{eff} and T_B values of complexes **8**,

9, **10** and **11** further support that movement of the oxygen atoms is linked with the magnetization relaxation in $[\text{L}_2\text{Dy}(\text{H}_2\text{O})_5]^{3+}$ family of SMMs.

In this manuscript, by analyzing the spin-phonon coupling, we have shown that the modulation of geometry via simple ligand substitution can shift the vibrations and decouple with the KD1-KD2 gap that is linked with the magnetization relaxation in **1-F**, **1-pCH₃**, **1-CH₃** and **5-CH₃** in comparison with the parent geometry **1**. As a result of this, an enhancement of U_{eff} and T_{B} values is observed compared to the parent complex. On the other hand, the electrostatic polarization of the donor atom strongly affects the spin-phonon coupling, as suggested by Lunghi and co-workers.⁴ They have demonstrated that employing a ligand system where the donor atom charges are not significantly affected by vibrations should lead to the potential SMM. In the case of complexes **2** and **3**, introducing a crown ether ligand in the equatorial position in place of five THF molecules minimizes the electronic delocalization, leading to the increase in the U_{eff} values. In the case of complex **4**, the replacement of -NH groups by oxygen also reduces the electronic delocalization; hence, a significant improvement in the U_{eff} value is observed in **4-N3O2** compared to **4**. It should be noted that the organometallic complex with haptic ligand and complexes with carbene ligand shows very high T_{B} values due to the minimal polarization in the first coordination sphere.

By leveraging the outcomes of spin-phonon calculations conducted on complexes **1-5**, a comprehensive analysis of the T_{B} values across all studied complexes has become possible, shedding particular light on the intriguingly low values observed in complexes **2** and **3**. It is worthwhile to mention that among complexes **1-5**, the largest T_{B} (FC/ZFC) value is observed for complex **5** (12 K), followed by **1** (9.5 K), **4** (5 K), and **2** \approx **3** (3.5 K). From these values, we can suggest that the T_{B} value is the lowest for complexes where the significant movement of metal and atoms in the first coordination controls the magnetization relaxation. This is the case with complexes **2** and **3**, where the vibration involving in-plane movement of the Dy ion is associated with the magnetization relaxation, and this is primarily due to the flexible first coordination sphere atoms. In the case of complex **4**, the atoms in the second coordination sphere, such as hydrogen atoms of -NH groups, control the magnetization relaxation. Therefore its T_{B} is slightly higher than complexes **2** and **3**. In the case of complex **1**, the hydrogen atoms associated with the phenyl and pyridine ring in the third coordination sphere govern the magnetization relaxation and result in larger T_{B} values compared to complexes **2**, **3** and **4**. Finally, in the case of complex **5**, the H-bonding interactions with the counter anions are linked with the magnetization relaxation. As the counter anions are involved in this case which is beyond the coordination sphere, this complex T_{B} value is the largest among all. Hence, the establishment of a rigid first coordination sphere surrounding Dy(III) is an imperative requirement when designing prospective SMMs. This should also be accompanied by a minimum electrostatic polarization of the corresponding donor atoms. Given the diverse nature of associated vibrations within this molecular class, a more extensive dataset encompassing all pseudo D_{5h} Dy(III) complexes, coupled with the power of AI/ML tools, holds tremendous potential to forge a path forward. Excitingly, this endeavor is currently underway in our laboratory.

5. Conclusions

In summary, by studying twenty-three molecules/models in the family of pseudo- D_{5h} Dy(III) Single-ion Magnets using DFT and *ab initio* CASSCF calculations, we have deciphered the large variation in the blocking temperature (T_B) observed in this class of molecules. The variation observed was attributed to the interplay between the spin-vibrational coupling and crystal field splitting of the ground state mJ level. The main conclusions drawn from our work are mentioned below:

(i) Predicting and enhancing the T_B by recognizing the vibration responsible for relaxation:

In [Dy(bbpen)Br] (**1**) complex and analogue structures with substitution on the ligand periphery (such as **1-F**, **1-pCH₃**, **1-pCH₃F**, **1-Cl**, **1-pCH₃(Cl)**, **1-Cl** and **1-pCH₃F(Cl)**), the ω_4 vibration which is corresponding to the vibrations of donor atoms at the first coordination sphere. This is due to the flexible coordination sphere provided by the ligand framework. Any chemical substitution that shifts this vibration is expected to enhance the T_B values. Quite interestingly, this coincides with a literature report where such substitution performed by a trial-and-error method was found to improve the T_B values, affirming faith in the model proposed. Armed with such outcomes, we further targeted the -CH₂ linkers that connect the amine nitrogen atom to the pyridinic ring at the equatorial positions and *in silico* models have been proposed to boost the T_B values further. A linear correlation between the difference in blocking temperature T_B and vibrational frequencies was observed, and this provides further means to predict the variation in the T_B values based on the shift in the computed frequencies.

(ii) Importance of equatorial ligand field in dictating T_B : Two complexes [Dy(OCMe₃)Br(THF)₅][BPh₄] (**2**) and [Dy(OSiMe₃)Br(THF)₅][BPh₄] (**3**) studied exhibit very low T_B values and these attributed to the vibration involving the asymmetric stretching of O-Dy-O bond along the axial direction coupled with inplane bending of the equatorial THF molecule. This is essentially due to the very weak equatorial coordination that provides enhanced axiality as desired but also offers low in-plane bendings, which causes magnetization relaxation reducing the T_B values. To arrest such movements, we have *in silico*-modelled geometries where a crown ether ligand replaced five THF molecules. This model is expected to boost the T_B value further. Studies on [Dy(L^{N5})(Ph₃SiO)₂](BPh₄).CH₂Cl₂ (**4**) reveal a similar scenario, and a suitable ligand substitution (N-H by O) was offered to boost the performance.

(iii) Controlling H-bonding Interactions to Improve T_B values: Our calculations on [L₂Dy(H₂O)₅][I]₃.L₂.H₂O (**5**) suggest that out-of-plane bending of the water molecules is one of the major factors in the relaxation mechanism. As these water molecules are in H-bonding interaction with the counteranions, efforts to modulate these vibrations will be proven to be beneficial. There are already literature reports where the T_B values were found to enhance if the equatorial planarity of the water molecules is improved via ligand design/cluster aggregation.

Through the meticulous execution of DFT and *ab initio* CASSCF calculations on a comprehensive set of twenty-three distinct Dy(III) pseudo D_{5h} complexes/models, we have successfully elucidated the underlying factors contributing to the significant variation in T_B values within this family. Moreover, we present a chemically viable methodology to fine-tune the performance of this intriguing molecular class for the first time.

6. Methodology

All the gas phase geometry optimizations and calculations of normal modes of complexes **1-5** were performed within the unrestricted DFT framework utilizing the Gaussian09 programme package.⁸² The X-ray structure (without counter anions and solvent molecules except in complex **5**) was employed as a starting point of geometry optimization. The hybrid B3LYP exchange-correlation functional (including dispersion corrections for **5**) was employed for the geometry optimization.⁸³⁻⁸⁵ The Dy(III) ion was replaced by Y(III) to aid smooth SCF convergence. We have used Stuttgart's effective core potential (SDD ECP, 28 core electrons) basis set for yttrium and iodine atoms.⁸⁶⁻⁸⁷ For other elements, a 6-31G* basis set was employed.⁸⁸ For the geometry optimization of model complexes, we have used SDD for yttrium and iodine, Ahlrichs triple- ζ plus polarization basis set for oxygen, nitrogen, fluorine and bromine and 6-31G* basis set for carbon and hydrogen atoms.⁸⁶⁻⁸⁹

All the *ab initio* CASSCF/RASSI-SO/SINGLE_ANISO calculations on the X-ray, optimized, and model complexes were performed using MOLCAS 8.2 programme package.⁹⁰ We have used Douglas-Kroll-Hess (DKH) Hamiltonian to take into account the relativistic effect of the metal centre.⁹¹ The Cholesky decomposition technique was used to reduce the size of the disk space.⁹² The basis sets of our calculations have been taken from ANO-RCC (Atomic natural orbital-relativistically core correlated) library available in MOLCAS. Here we have used the VTZP quality basis set for Dy, the VDZP quality basis set for the atoms in the first coordination sphere, and the VDZ quality basis set for the atoms from the secondary coordination sphere onwards. The active space for the complete active space self-consistent field (CASSCF) calculations consists of nine 4f electrons in seven 4f orbitals of Dy(III). We have performed state average CASSCF calculations for the twenty-one sextets of Dy(III) ions. The quartet and doublet spin states of Dy(III) were not considered in our calculations to reduce the computational cost since they do not contribute significantly to the spin-orbit energies, as seen from earlier studies. However, the twenty-one spin-free states were mixed by spin-orbit coupling in the RASSI-SO module. Thereafter, the SINGLE_ANISO module was used to compute the g-tensors, crystal field parameters, magnetic properties such as susceptibility, QTM and TA-QTM etc.

Computational Procedures for spin-phonon relaxation: The vibrational modes of a complex were determined from the geometry optimization in the gas phase within the DFT framework. Frequency calculations were utilized to confirm that the optimized geometries are true minima in the potential energy surface. We have used uncalibrated frequencies to interpret magnetization relaxation dynamics because experimental IR spectra were not available for low-energy vibrational modes. It should be noted that uncalibrated frequencies are generally found to be smaller than calibrated frequencies due to the gas-phase optimization and smaller reduced mass of yttrium compared to dysprosium.^{46, 48}

The distorted geometries for each vibrational mode are computed as⁹³⁻⁹⁴:

$$q_n = q_{eq} + n \cdot q_p \quad (1)$$

where, q_n is the distorted geometry, q_e is the equilibrium geometry, n is the employed finite distortion and q_p is the displacement vector of each mode.

The value of n was extracted from the definition of harmonic oscillator approximation:

$$\frac{1}{2}kn^2 = \frac{1}{2}\hbar\omega \quad (2)$$

where k , \hbar and ω represent the force constant of each vibrational mode, Planck constant and angular frequency, respectively. Then considering this approximation, we have calculated the maximum finite displacement of each vibrational mode.

After geometry optimization, we performed CASSCF/RASSI-SO/SINGLE_ANISO calculations at four displacements of selected ten high-intensity vibrational modes. The crystal field (CF) parameters from the *ab initio* calculations were obtained with the Iwahara-Chibotaru definition,⁹⁵⁻⁹⁶

$$\hat{H}_{CF} = \sum_{kq} B_k^q \hat{O}_k^q(\hat{J}) = \sum_{kq} B_k^q \frac{\hat{O}_{kq}^S(\hat{J})}{O_{ko}^S(J)} \quad (3)$$

Here, B_k^q represents the CF parameters and the $O_{ko}^S(J)$ was obtained from $\hat{O}_{kq}^S(\hat{J})$ (Stevens operator) with the replacement of $\hat{J}_Z = J$. The k , referred to as ranks, runs to $2J$. The components of q range from $-k$ to $+k$ for each k . The main advantage of the Iwahara-Chibotaru definition compared to Stevens notation is the CF parameters are symmetric in the former, $|B_k^q| = |B_k^{-q}|$. However, we are mostly interested in the magnitude of the CF parameters that are entered in the transition probabilities (*vide infra*). The electronic part of the spin-phonon coupling Hamiltonian has a contribution from the first and second-order contributions from optical phonons that are expressed as^{95,97}

$$\hat{H}_{sp}^{(1)} = \sum_n x_j \sum_{kq} \left. \frac{\partial B_k^q}{\partial x_j} \right|_{x_j=0} \hat{O}_k^q(\hat{J}) \quad (4)$$

$$\hat{H}_{sp}^{(2)} = \sum_{ij} x_j x_j \sum_{kq} \left. \frac{\partial^2 B_k^q}{\partial x_i \partial x_j} \right|_{x_i, x_j=0} \hat{O}_k^q(\hat{J}) \quad (5)$$

s

$$P(\psi \leftarrow \psi') = \frac{2\pi}{\hbar^2} \left| \langle \psi | \hat{H}_{sp}^{(1)} | \psi' \rangle \right|^2 f(\omega), \quad (6)$$

$$P(\psi \leftarrow \psi') = \frac{2\pi}{\hbar^2} \left| \langle \psi | \hat{H}_{sp}^{(2)} | \psi' \rangle \right|^2 f(\omega), \text{ and} \quad (7)$$

$$P(\psi \leftarrow \psi') = \frac{2\pi}{\hbar^2} \left| \frac{\langle \psi | \hat{H}_{sp}^{(1)} | \psi' \rangle \langle \psi' | \hat{H}_{sp}^{(1)} | \psi \rangle}{\Delta} \right|^2 f(\omega), \quad (8)$$

Here, $f(\omega)$ is a factor, the value of which depends on the vibrational modes and the energy difference between the states $|\psi\rangle$ and $|\psi'\rangle$. \hbar is the reduced Planck constant. $|\psi'\rangle$ represents the intermediate state for the Raman process and Δ is the energy difference of this state with the initial state. The Orbach process is represented by several consecutive direct transitions. Hence the transition probability of the Orbach process is proportional to the spin-phonon coupling Hamiltonian.

The lowest two KDs of the chosen Dy(III) SIMs in our study are found to have a large projection on $|J, M_J\rangle$ states. Therefore, we can express the two CF states $|\psi\rangle$ and $|\psi'\rangle$ as pure $|J, M_J\rangle$ states; $|\psi\rangle \sim |J, M_J\rangle$ and $|\psi'\rangle \sim |J, M_J'\rangle$.⁴⁸ The $\hat{O}_2^{\pm 1}(J)$ operators promote direct transitions between $|J, M_J\rangle$ states that differ by $\Delta M_J = M_J' - M_J = \pm 1$. If we confine ourselves into the lowest two KDs, the $\Delta M_J = \pm 1$ should correspond to the transition from $|\frac{15}{2}, \pm \frac{15}{2}\rangle \rightarrow |\frac{15}{2}, \pm \frac{13}{2}\rangle$. According to the eqns (2) and (4), the normal modes for $\Delta M_J = \pm 1$ transition should correspond to large $\left|\frac{\partial B_2^{\pm 1}}{\partial x_j}\right|^2$ value. On the other hand, these normal modes should lie between the energy of the KD1 and KD2. It should be noted that the largest derivatives are obtained from the 2nd rank parameters, and therefore we will confine ourselves within 2nd rank parameters to understand the Orbach relaxation process.

Furthermore, the earlier spin dynamics study on "dysprosocenium" complexes reveals that normal modes that cause the $|\frac{15}{2}, \pm \frac{15}{2}\rangle \rightarrow |\frac{15}{2}, \pm \frac{13}{2}\rangle$ possess $\left|\frac{\partial B_2^{\pm 1}}{\partial x_j}\right|^2 > 1000$.⁴⁸ Therefore, we will focus on finding the normal vibrational modes with large $\left|\frac{\partial B_2^{\pm 1}}{\partial x_j}\right|^2$ value in our study ($|B_2^{+1}| = |B_2^{-1}|$, according to Iwahara-Chibotaru definition). On the other hand, the factor $f(\omega)$ depends on the phonon density of states of vibrational modes.⁴⁸ Therefore, we have performed spin-phonon coupling calculations on selected vibrational modes possessing significant oscillator strength to reduce the computational cost. Furthermore, the earlier studies on "dysprosocenium" complexes also indicated that the vibrational modes causing $|\frac{15}{2}, \pm \frac{15}{2}\rangle \rightarrow |\frac{15}{2}, \pm \frac{13}{2}\rangle$ has a significant IR intensity supporting the approach adapted here to reduce the computational cost.^{46, 48}

The thermal evolution of CF parameter (B) is calculated using a Grand Canonical Ensemble as follows,⁹³⁻⁹⁴

$$\langle \bar{B} \rangle (T) \approx \langle \bar{B} \rangle (T = 0) + \sum_{k=1}^R \left[\frac{\hbar}{4\pi} \left(\frac{\partial^2 B}{\partial q^2} \right)_e \frac{1}{m_k \omega_k} \langle n_k \rangle \right] \quad (9)$$

where $\langle \bar{B} \rangle (T = 0)$ and $\langle n_k \rangle$ are represented as,

$$\langle \bar{B} \rangle (T = 0) = (B)_e + \sum_{k=1}^R \left[\frac{\hbar}{4\pi} \left(\frac{\partial^2 B}{\partial q^2} \right)_e \frac{1}{m_k \omega_k} \right] \quad (10)$$

$$\langle B_k \rangle = \frac{1}{e^{\frac{\hbar \omega_k}{k_B T}} - 1}$$

where B_e is the CF parameter of undistorted geometry, m_k and ω_k are the reduced mass and frequency of vibrational mode k.

The right-hand side of eqn. 10 is made of the product of a factor that represents the coupling strength of a given mode and a temperature-dependent part, the boson number (B_k) which

characterizes the thermal population of a mode. The coupling strength of a given vibrational mode is defined as follows⁹³⁻⁹⁴:

$$C_k = \frac{\hbar}{4\pi} \left(\frac{\partial^2 B}{\partial q^2} \right)_e \frac{1}{m_k \omega_k} \quad (11)$$

Supporting Information

The Supporting Information is available free of charge at XXXXXXXXXXXX. This contains structural parameters in optimized versus crystal structures, tables containing *ab initio* calculated parameters, additional figures, optimized geometries, frequencies, reduced masses and force constants of the various normal modes of vibrations, computed crystal field parameters, computed IR spectrum, optimized coordinates of the complexes.

Acknowledgement

We thank IIT Bombay for its supercomputing facility. S.D thanks to IIT Bombay for IPDF fellowship. G.R. would like to acknowledge DST and SERB (CRG/2018/00430; SB/SJF/2019-20/12; and SPR/2019/001145) for funding. TS is thankful to CSIR for the fellowship.

References:

1. Lunghi, A.; Totti, F.; Sanvito, S.; Sessoli, R., Intra-molecular origin of the spin-phonon coupling in slow-relaxing molecular magnets. *Chem. Sci.* **2017**, *8* (9), 6051-6059.
2. Lunghi, A.; Totti, F.; Sessoli, R.; Sanvito, S., The role of anharmonic phonons in under-barrier spin relaxation of single molecule magnets. *Nat. Commun.* **2017**, *8* (1), 1-7.
3. Lunghi, A.; Sanvito, S., Multiple spin-phonon relaxation pathways in a Kramer single-ion magnet. *J. Chem. Phys.* **2020**, *153* (17), 174113.
4. Briganti, M.; Santanni, F.; Tesi, L.; Totti, F.; Sessoli, R.; Lunghi, A., A Complete Ab Initio View of Orbach and Raman Spin-Lattice Relaxation in a Dysprosium Coordination Compound. *J. Am. Chem. Soc.* **2021**, *143* (34), 13633-13645.
5. Reta, D.; Kragoskow, J. G. C.; Chilton, N. F., Ab Initio Prediction of High-Temperature Magnetic Relaxation Rates in Single-Molecule Magnets. *J. Am. Chem. Soc.* **2021**, *143* (15), 5943-5950.
6. Gould, C. A.; McClain, K. R.; Reta, D.; Kragoskow, J. G.; Marchiori, D. A.; Lachman, E.; Choi, E.-S.; Analytis, J. G.; Britt, R. D.; Chilton, N. F., Ultrahard magnetism from mixed-valence dylanthanide complexes with metal-metal bonding. *Science* **2022**, *375* (6577), 198-202.
7. Kragoskow, J. G.; Marbey, J.; Buch, C. D.; Nehrkorn, J.; Ozerov, M.; Piligkos, S.; Hill, S.; Chilton, N. F., Analysis of vibronic coupling in a 4f molecular magnet with FIRMS. *Nat. Commun.* **2022**, *13* (1), 1-10.
8. Escalera-Moreno, L.; Baldoví, J. J.; Gaita-Ariño, A.; Coronado, E., Spin states, vibrations and spin relaxation in molecular nanomagnets and spin qubits: a critical perspective. *Chem. Sci.* **2018**, *9* (13), 3265-3275.
9. Escalera-Moreno, L.; Baldoví, J. J.; Gaita-Ariño, A.; Coronado, E., Design of high-temperature f-block molecular nanomagnets through the control of vibration-induced spin relaxation. *Chem. Sci.* **2020**, *11* (6), 1593-1598.
10. Bar, A. K.; Kalita, P.; Singh, M. K.; Rajaraman, G.; Chandrasekhar, V., Low-coordinate mononuclear lanthanide complexes as molecular nanomagnets. *Coord. Chem. Rev.* **2018**, *367*, 163-216.
11. McAdams, S. G.; Ariciu, A.-M.; Kostopoulos, A. K.; Walsh, J. P.; Tuna, F., Molecular single-ion magnets based on lanthanides and actinides: Design considerations and new advances in the context of quantum technologies. *Coord. Chem. Rev.* **2017**, *346*, 216-239.
12. Liddle, S. T.; van Slageren, J., Improving f-element single molecule magnets. *Chem. Soc. Rev.* **2015**, *44* (19), 6655-6669.
13. Ishikawa, N.; Sugita, M.; Ishikawa, T.; Koshihara, S.-y.; Kaizu, Y., Lanthanide double-decker complexes functioning as magnets at the single-molecular level. *J. Am. Chem. Soc.* **2003**, *125* (29), 8694-8695.
14. Blagg, R. J.; Ungur, L.; Tuna, F.; Speak, J.; Comar, P.; Collison, D.; Wernsdorfer, W.; McInnes, E. J.; Chibotaru, L. F.; Winpenny, R. E., Magnetic relaxation pathways in lanthanide single-molecule magnets. *Nat. Chem.* **2013**, *5* (8), 673-678.

15. Blagg, R. J.; Muryn, C. A.; McInnes, E. J.; Tuna, F.; Winpenny, R. E., Single pyramid magnets: Dy⁵ pyramids with slow magnetic relaxation to 40 K. *Angew. Chem. Int. Ed.* **2011**, *123* (29), 6660-6663.
16. Blagg, R. J.; Tuna, F.; McInnes, E. J.; Winpenny, R. E., Pentametallic lanthanide-alkoxide square-based pyramids: high energy barrier for thermal relaxation in a holmium single molecule magnet. *Chem. Comm.* **2011**, *47* (38), 10587-10589.
17. Ungur, L.; Le Roy, J. J.; Korobkov, I.; Murugesu, M.; Chibotaru, L. F., Fine-tuning the local symmetry to attain record blocking temperature and magnetic remanence in a single-ion magnet. *Angew. Chem. Int. Ed.* **2014**, *126* (17), 4502-4506.
18. Jiang, S.-D.; Wang, B.-W.; Sun, H.-L.; Wang, Z.-M.; Gao, S., An organometallic single-ion magnet. *J. Am. Chem. Soc.* **2011**, *133* (13), 4730-4733.
19. Le Roy, J. J.; Korobkov, I.; Murugesu, M., A sandwich complex with axial symmetry for harnessing the anisotropy in a prolate erbium (III) ion. *Chem. Comm.* **2014**, *50* (13), 1602-1604.
20. Le Roy, J. J.; Jeletic, M.; Gorelsky, S. I.; Korobkov, I.; Ungur, L.; Chibotaru, L. F.; Murugesu, M., An organometallic building block approach to produce a multidecker 4 f single-molecule magnet. *J. Am. Chem. Soc.* **2013**, *135* (9), 3502-3510.
21. Demir, S.; Zadrozny, J. M.; Long, J. R., Large Spin-Relaxation Barriers for the Low-Symmetry Organolanthanide Complexes [Cp*₂Ln(BPh₄)](Cp* = pentamethylcyclopentadienyl; Ln = Tb, Dy). *Chem. Eur. J.* **2014**, *20* (31), 9524-9529.
22. Brown, A. J.; Pinkowicz, D.; Saber, M. R.; Dunbar, K. R., A Trigonal-Pyramidal Erbium (III) Single-Molecule Magnet. *Angew. Chem. Int. Ed.* **2015**, *127* (20), 5962-5966.
23. Zhang, P.; Zhang, L.; Wang, C.; Xue, S.; Lin, S.-Y.; Tang, J., Equatorially coordinated lanthanide single ion magnets. *J. Am. Chem. Soc.* **2014**, *136* (12), 4484-4487.
24. Tanaka, D.; Inose, T.; Tanaka, H.; Lee, S.; Ishikawa, N.; Ogawa, T., Proton-induced switching of the single molecule magnetic properties of a porphyrin based Tb III double-decker complex. *Chem. Comm.* **2012**, *48* (63), 7796-7798.
25. Batchelor, L. J.; Cimatti, I.; Guillot, R.; Tuna, F.; Wernsdorfer, W.; Ungur, L.; Chibotaru, L. F.; Campbell, V. E.; Mallah, T., Chemical tuning of the magnetic relaxation in dysprosium (III) mononuclear complexes. *Dalton Trans.* **2014**, *43* (32), 12146-12149.
26. Mondal, A. K.; Goswami, S.; Konar, S., Influence of the coordination environment on slow magnetic relaxation and photoluminescence behavior in two mononuclear dysprosium (III) based single molecule magnets. *Dalton Trans.* **2015**, *44* (11), 5086-5094.
27. Cao, W.; Gao, C.; Zhang, Y.-Q.; Qi, D.; Liu, T.; Wang, K.; Duan, C.; Gao, S.; Jiang, J., Rational enhancement of the energy barrier of bis (tetrapyrrole) dysprosium SMMs via replacing atom of porphyrin core. *Chem. Sci.* **2015**, *6* (10), 5947-5954.
28. Liu, S.-S.; Lang, K.; Zhang, Y.-Q.; Yang, Q.; Wang, B.-W.; Gao, S., A distinct magnetic anisotropy enhancement in mononuclear dysprosium-sulfur complexes by controlling the Dy-ligand bond length. *Dalton Trans.* **2016**, *45* (19), 8149-8153.
29. Yu, K.-X.; Ding, Y.-S.; Han, T.; Leng, J.-D.; Zheng, Y.-Z., Magnetic relaxations in four-coordinate Dy (iii) complexes: effects of anionic surroundings and short Dy-O bonds. *Inorg. Chem. Front.* **2016**, *3* (8), 1028-1034.
30. Wang, Y.-L.; Ma, Y.; Yang, X.; Tang, J.; Cheng, P.; Wang, Q.-L.; Li, L.-C.; Liao, D.-Z., Syntheses, structures, and magnetic and luminescence properties of a new DyIII-based single-ion magnet. *Inorg. Chem.* **2013**, *52* (13), 7380-7386.
31. Campbell, V. E.; Bolvin, H.; Rivière, E.; Guillot, R.; Wernsdorfer, W.; Mallah, T., Structural and electronic dependence of the single-molecule-magnet behavior of dysprosium (III) complexes. *Inorg. Chem.* **2014**, *53* (5), 2598-2605.
32. Jiang, S. D.; Wang, B. W.; Su, G.; Wang, Z. M.; Gao, S., A Mononuclear Dysprosium Complex Featuring Single-Molecule-Magnet Behavior. *Angew. Chem. Int. Ed.* **2010**, *122* (41), 7610-7613.
33. Chen, G.-J.; Gao, C.-Y.; Tian, J.-L.; Tang, J.; Gu, W.; Liu, X.; Yan, S.-P.; Liao, D.-Z.; Cheng, P., Coordination-perturbed single-molecule magnet behaviour of mononuclear dysprosium complexes. *Dalton Trans.* **2011**, *40* (20), 5579-5583.
34. Chen, G. J.; Guo, Y. N.; Tian, J. L.; Tang, J.; Gu, W.; Liu, X.; Yan, S. P.; Cheng, P.; Liao, D. Z., Enhancing anisotropy barriers of dysprosium (III) single-ion magnets. *Chem. Eur. J.* **2012**, *18* (9), 2484-2487.
35. Gupta, S. K.; Rajeshkumar, T.; Rajaraman, G.; Murugavel, R., An air-stable Dy(III) single-ion magnet with high anisotropy barrier and blocking temperature. *Chem. Sci.* **2016**, *7* (8), 5181-5191.
36. Chen, Y.-C.; Liu, J.-L.; Ungur, L.; Liu, J.; Li, Q.-W.; Wang, L.-F.; Ni, Z.-P.; Chibotaru, L. F.; Chen, X.-M.; Tong, M.-L., Symmetry-supported magnetic blocking at 20 K in pentagonal bipyramidal Dy (III) single-ion magnets. *J. Am. Chem. Soc.* **2016**, *138* (8), 2829-2837.

37. Ding, Y. S.; Chilton, N. F.; Winpenny, R. E.; Zheng, Y. Z., On approaching the limit of molecular magnetic anisotropy: a near-perfect pentagonal bipyramidal dysprosium (III) single-molecule magnet. *Angew. Chem. Int. Ed.* **2016**, *55* (52), 16071-16074.
38. Liu, J.; Chen, Y.-C.; Liu, J.-L.; Vieru, V.; Ungur, L.; Jia, J.-H.; Chibotaru, L. F.; Lan, Y.; Wernsdorfer, W.; Gao, S., A stable pentagonal bipyramidal Dy (III) single-ion magnet with a record magnetization reversal barrier over 1000 K. *J. Am. Chem. Soc.* **2016**, *138* (16), 5441-5450.
39. Zhu, L.; Yin, B.; Ma, P.; Li, D., Tuning the equatorial crystal-field in mononuclear DyIII complexes to improve single-molecule magnetic properties. *Inorg. Chem.* **2020**, *59* (22), 16117-16121.
40. Li, M.; Wu, H.; Yang, Q.; Ke, H.; Yin, B.; Shi, Q.; Wang, W.; Wei, Q.; Xie, G.; Chen, S., Experimental and Theoretical Interpretation on the Magnetic Behavior in a Series of Pentagonal-Bipyramidal DyIII Single-Ion Magnets. *Chem. Eur. J.* **2017**, *23* (70), 17775-17787.
41. Zhang, S.; Wu, H.; Sun, L.; Ke, H.; Chen, S.; Yin, B.; Wei, Q.; Yang, D.; Gao, S., Ligand field fine-tuning on the modulation of the magnetic properties and relaxation dynamics of dysprosium(III) single-ion magnets (SIMs): synthesis, structure, magnetism and ab initio calculations. *J. Mater. Chem. C* **2017**, *5* (6), 1369-1382.
42. Jiang, Z.; Sun, L.; Yang, Q.; Yin, B.; Ke, H.; Han, J.; Wei, Q.; Xie, G.; Chen, S., Excess axial electrostatic repulsion as a criterion for pentagonal bipyramidal Dy III single-ion magnets with high Ueff and TB. *J. Mater. Chem. C* **2018**, *6* (15), 4273-4280.
43. Ding, Y. S.; Han, T.; Zhai, Y. Q.; Reta, D.; Chilton, N. F.; Winpenny, R. E.; Zheng, Y. Z., A Study of Magnetic Relaxation in Dysprosium (III) Single-Molecule Magnets. *Chem. Eur. J.* **2020**, *26* (26), 5893-5902.
44. Tesi, L.; Lunghi, A.; Atzori, M.; Lucaccini, E.; Sorace, L.; Totti, F.; Sessoli, R., Giant spin-phonon bottleneck effects in evaporable vanadyl-based molecules with long spin coherence. *Dalton Trans.* **2016**, *45* (42), 16635-16643.
45. Atzori, M.; Tesi, L.; Benci, S.; Lunghi, A.; Righini, R.; Taschin, A.; Torre, R.; Sorace, L.; Sessoli, R., Spin dynamics and low energy vibrations: insights from vanadyl-based potential molecular qubits. *J. Am. Chem. Soc.* **2017**, *139* (12), 4338-4341.
46. Goodwin, C. A. P.; Ortu, F.; Reta, D.; Chilton, N. F.; Mills, D. P., Molecular magnetic hysteresis at 60 kelvin in dysprosocenium. *Nature* **2017**, *548* (7668), 439-442.
47. Guo, F. S.; Day, B. M.; Chen, Y. C.; Tong, M. L.; Mansikkamäki, A.; Layfield, R. A., A dysprosium metallocene single-molecule magnet functioning at the axial limit. *Angew. Chem. Int. Ed.* **2017**, *129* (38), 11603-11607.
48. Guo, F.-S.; Day, B. M.; Chen, Y.-C.; Tong, M.-L.; Mansikkamäki, A.; Layfield, R. A., Magnetic hysteresis up to 80 kelvin in a dysprosium metallocene single-molecule magnet. *Science* **2018**, *362* (6421), 1400-1403.
49. McClain, K. R.; Gould, C. A.; Chakarawet, K.; Teat, S. J.; Groshens, T. J.; Long, J. R.; Harvey, B. G., High-temperature magnetic blocking and magneto-structural correlations in a series of dysprosium (III) metallocenium single-molecule magnets. *Chem. Sci.* **2018**, *9* (45), 8492-8503.
50. Lunghi, A.; Sanvito, S., How do phonons relax molecular spins? *Science advances* **2019**, *5* (9), eaax7163.
51. Lunghi, A., Insights into the Spin-Lattice Dynamics of Organic Radicals Beyond Molecular Tumbling: A Combined Molecular Dynamics and Machine-Learning Approach. *Applied Magnetic Resonance* **2020**, *51* (11), 1343-1356.
52. Nabi, R.; Kragsskow, J.; Staab, J.; Reta, D.; Skelton, J.; Chilton, N., Impact of Finite Phonon Lifetimes on the Spin Dynamics of Single-Molecule Magnets. **2023**.
53. Mondal, S.; Lunghi, A., Unraveling the Contributions to Spin-Lattice Relaxation in Kramers Single-Molecule Magnets. *J. Am. Chem. Soc.* **2022**.
54. Albino, A.; Benci, S.; Tesi, L.; Atzori, M.; Torre, R.; Sanvito, S.; Sessoli, R.; Lunghi, A., First-Principles Investigation of Spin-Phonon Coupling in Vanadium-Based Molecular Spin Quantum Bits. *Inorg. Chem.* **2019**, *58* (15), 10260-10268.
55. Liu, J.-L.; Chen, Y.-C.; Zheng, Y.-Z.; Lin, W.-Q.; Ungur, L.; Wernsdorfer, W.; Chibotaru, L. F.; Tong, M.-L., Switching the anisotropy barrier of a single-ion magnet by symmetry change from quasi-D5h to quasi-O_h. *Chem. Sci.* **2013**, *4* (8), 3310-3316.
56. Chen, Y. C.; Liu, J. L.; Lan, Y.; Zhong, Z. Q.; Mansikkamäki, A.; Ungur, L.; Li, Q. W.; Jia, J. H.; Chibotaru, L. F.; Han, J. B.; Wernsdorfer, W.; Chen, X. M.; Tong, M. L., Dynamic Magnetic and Optical Insight into a High Performance Pentagonal Bipyramidal Dy(III) Single-Ion Magnet. *Chem. Eur. J.* **2017**, *23* (24), 5708-5715.
57. Canaj, A. B.; Singh, M. K.; Wilson, C.; Rajaraman, G.; Murrie, M., Chemical and in silico tuning of the magnetization reversal barrier in pentagonal bipyramidal Dy (iii) single-ion magnets. *Chem. Comm.* **2018**, *54* (59), 8273-8276.
58. Canaj, A. B.; Dey, S.; Wilson, C.; Cespedes, O.; Rajaraman, G.; Murrie, M., Engineering macrocyclic high performance pentagonal bipyramidal Dy(III) single-ion magnets. *Chem. Comm.* **2020**, *56* (80), 12037-12040.

59. Sarkar, A.; Rajaraman, G., Modulating magnetic anisotropy in Ln (III) single-ion magnets using an external electric field. *Chem. Sci.* **2020**, *11* (38), 10324-10330.
60. Ding, Y.-S.; Yu, K.-X.; Reta, D.; Ortu, F.; Winpenny, R. E.; Zheng, Y.-Z.; Chilton, N. F., Field-and temperature-dependent quantum tunnelling of the magnetization in a large barrier single-molecule magnet. *Nat. Commun.* **2018**, *9* (1), 1-10.
61. Li, Z.-H.; Zhai, Y.-Q.; Chen, W.-P.; Luo, Q.-C.; Han, T.; Zheng, Y.-Z., Breaking the axiality of pentagonal-bipyramidal dysprosium (III) single-molecule magnets with pyrazolate ligands. *Inorg. Chem. Front.* **2020**, *7* (22), 4367-4376.
62. Kalita, P.; Ahmed, N.; Bar, A. K.; Dey, S.; Jana, A.; Rajaraman, G.; Sutter, J.-P.; Chandrasekhar, V., Pentagonal Bipyramidal Ln (III) Complexes Containing an Axial Phosphine Oxide Ligand: Field-induced Single-ion Magnetism Behavior of the Dy (III) Analogues. *Inorg. Chem.* **2020**, *59* (9), 6603-6612.
63. Díaz-Ortega, I. F.; Herrera, J. M.; Dey, S.; Nojiri, H.; Rajaraman, G.; Colacio, E., The effect of the electronic structure and flexibility of the counteranions on magnetization relaxation in [Dy (L) 2 (H 2 O) 5] 3+(L= phosphine oxide derivative) pentagonal bipyramidal SIMs. *Inorg. Chem. Front.* **2020**, *7* (3), 689-699.
64. Norre, M. S.; Gao, C.; Dey, S.; Gupta, S. K.; Borah, A.; Murugavel, R.; Rajaraman, G.; Overgaard, J., High-Pressure Crystallographic and Magnetic Studies of Pseudo-D5h Symmetric Dy(III) and Ho(III) Single-Molecule Magnets. *Inorg. Chem.* **2020**, *59* (1), 717-729.
65. Bar, A. K.; Kalita, P.; Sutter, J.-P.; Chandrasekhar, V., Pentagonal-bipyramid Ln (III) complexes exhibiting single-ion-magnet behavior: a rational synthetic approach for a rigid equatorial plane. *Inorg. Chem.* **2018**, *57* (5), 2398-2401.
66. Gupta, S. K.; Dey, S.; Rajeshkumar, T.; Rajaraman, G.; Murugavel, R., Deciphering the Role of Anions and Secondary Coordination Sphere in Tuning Anisotropy in Dy(III) Air-Stable D5h SIMs. *Chem. Eur. J.*, **2022**, *28* (4), e202103585.
67. Yu, K.-X.; Kragoskow, J. G.; Ding, Y.-S.; Zhai, Y.-Q.; Reta, D.; Chilton, N. F.; Zheng, Y.-Z., Enhancing magnetic hysteresis in single-molecule magnets by ligand functionalization. *Chem* **2020**, *6* (7), 1777-1793.
68. Canaj, A. B.; Dey, S.; Wilson, C.; Céspedes, O.; Rajaraman, G.; Murrie, M., Engineering macrocyclic high performance pentagonal bipyramidal Dy (iii) single-ion magnets. *Chem. Comm.* **2020**, *56* (80), 12037-12040.
69. Zhu, L.; Dong, Y.; Yin, B.; Ma, P.; Li, D., Improving the single-molecule magnet properties of two pentagonal bipyramidal Dy³⁺ compounds by the introduction of both electron-withdrawing and-donating groups. *Dalton Trans.* **2021**, *50* (36), 12607-12618.
70. Tesi, L.; Salman, Z.; Cimatti, I.; Pointillart, F.; Bernot, K.; Mannini, M.; Sessoli, R., Isotope effects on the spin dynamics of single-molecule magnets probed using muon spin spectroscopy. *Chem. Comm.* **2018**, *54* (56), 7826-7829.
71. Zabala-Lekuona, A.; Seco, J. M.; Colacio, E., Single-Molecule Magnets: From Mn¹²-ac to dysprosium metallocenes, a travel in time. *Coord. Chem. Rev.* **2021**, *441*, 213984.
72. Huang, G.; Yi, X.; Jung, J.; Guillou, O.; Cador, O.; Pointillart, F.; Le Guennic, B.; Bernot, K., Optimization of Magnetic Relaxation and Isotopic Enrichment in Dimeric DyIII Single-Molecule Magnets. *Eur. J. Inorg. Chem.* **2018**, *2018* (3-4), 326-332.
73. Wada, H.; Ooka, S.; Yamamura, T.; Kajiwara, T., Light lanthanide complexes with crown ether and its aza derivative which show slow magnetic relaxation behaviors. *Inorg. Chem.* **2017**, *56* (1), 147-155.
74. Maxwell, L.; Amozá, M.; Ruiz, E., Mononuclear lanthanide complexes with 18-crown-6 ether: synthesis, characterization, magnetic properties, and theoretical studies. *Inorg. Chem.* **2018**, *57* (21), 13225-13234.
75. Borah, A.; Dey, S.; Gupta, S. K.; Rajaraman, G.; Murugavel, R., Field-Induced SIM Behaviour in Early Lanthanide(III) Organophosphates Incorporating 18-crown-6. *Dalton Trans.* **2023**.
76. Gupta, S. K.; Dey, S.; Rajeshkumar, T.; Rajaraman, G.; Murugavel, R., Deciphering the Role of Anions and Secondary Coordination Sphere in Tuning Anisotropy in Dy (III) Air-Stable D5h SIMs. *Chem. Eur. J.* **2022**, *28* (4), e202103585.
77. Qu, Y.-X.; Ruan, Z.-Y.; Lyu, B.-H.; Chen, Y.-C.; Huang, G.-Z.; Liu, J.-L.; Tong, M.-L., Opening magnetic hysteresis via improving the planarity of equatorial coordination by hydrogen bonding. *Dalton Trans.* **2022**.
78. Lunghi, A.; Sanvito, S., Computational design of magnetic molecules and their environment using quantum chemistry, machine learning and multiscale simulations. *Nat. Rev. Chem.* **2022**, *6* (11), 761-781.
79. Mondal, S.; Lunghi, A., Spin-phonon decoherence in solid-state paramagnetic defects from first principles. *arXiv preprint arXiv:2212.11705* **2022**.
80. Lunghi, A., Spin-phonon relaxation in magnetic molecules: theory, predictions and insights. *arXiv preprint arXiv:2202.03776* **2022**.
81. Murugavel, R.; Gupta, S. K.; Dey, S.; Rajeshkumar, T.; Rajaraman, G., Deciphering the role of anions and secondary coordination sphere in tuning anisotropy in Dy (III) air-stable D5h SIMs. *Chem. Eur. J.* **2021**.
82. Gaussian 09, Revision A.02, M. J. Frisch, G. W. Trucks, H. B. Schlegel, G. E. Scuseria, M. A. Robb, J. R. Cheeseman, G. Scalmani, V. Barone, B. Mennucci, G. A. Petersson, H. Nakatsuji, M. Caricato, X. Li, H. P.

- Hratchian, A. F. Izmaylov, J. Bloino, G. Zheng, J. L. Sonnenberg, M. Hada, M. Ehara, K. Toyota, R. Fukuda, J. Hasegawa, M. Ishida, T. Nakajima, Y. Honda, O. Kitao, H. Nakai, T. Vreven, J. A. Montgomery, Jr., J. E. Peralta, F. Ogliaro, M. Bearpark, J. J. Heyd, E. Brothers, K. N. Kudin, V. N. Staroverov, R. Kobayashi, J. Normand, K. Raghavachari, A. Rendell, J. C. Burant, S. S. Iyengar, J. Tomasi, M. Cossi, N. Rega, J. M. Millam, M. Klene, J. E. Knox, J. B. Cross, V. Bakken, C. Adamo, J. Jaramillo, R. Gomperts, R. E. Stratmann, O. Yazyev, A. J. Austin, R. Cammi, C. Pomelli, J. W. Ochterski, R. L. Martin, K. Morokuma, V. G. Zakrzewski, G. A. Voth, P. Salvador, J. J. Dannenberg, S. Dapprich, A. D. Daniels, O. Farkas, J. B. Foresman, J. V. Ortiz, J. Cioslowski, and D. J. Fox, Gaussian, Inc., Wallingford CT, 2009.
83. Becke, A. D., Density-functional thermochemistry. III. The role of exact exchange. *J. Chem. Phys.* **1993**, *98* (7), 5648-5652.
84. Grimme, S.; Antony, J.; Ehrlich, S.; Krieg, H., A consistent and accurate ab initio parametrization of density functional dispersion correction (DFT-D) for the 94 elements H-Pu. *J. Chem. Phys.* **2010**, *132* (15), 154104.
85. Grimme, S., Semiempirical GGA-type density functional constructed with a long-range dispersion correction. *J. Comput. Chem.* **2006**, *27* (15), 1787-1799.
86. Cao, X.; Dolg, M., Segmented contraction scheme for small-core lanthanide pseudopotential basis sets. *Journal of Molecular Structure: THEOCHEM* **2002**, *581* (1-3), 139-147.
87. Cao, X., THEOCHEM 2002, 581, 139.(b) Cao, X.; Dolg, M. *J. Chem. Phys.* **2001**, *115*, 7348.
88. Rassolov, V. A.; Pople, J. A.; Ratner, M. A.; Windus, T. L., 6-31G* basis set for atoms K through Zn. *J. Chem. Phys.* **1998**, *109* (4), 1223-1229.
89. Schäfer, A.; Horn, H.; Ahlrichs, R., Fully optimized contracted Gaussian basis sets for atoms Li to Kr. *J. Chem. Phys.* **1992**, *97* (4), 2571-2577.
90. Aquilante, F.; Autschbach, J.; Carlson, R. K.; Chibotaru, L. F.; Delcey, M. G.; De Vico, L.; Fdez. Galván, I.; Ferré, N.; Frutos, L. M.; Gagliardi, L., Molcas 8: New capabilities for multiconfigurational quantum chemical calculations across the periodic table. *J. Comput. Chem.* **2016**, *37* (5), 506-541.
91. Reiher, M., Douglas–Kroll–Hess Theory: a relativistic electrons-only theory for chemistry. *Theo. Chem. Acs.* **2006**, *116* (1), 241-252.
92. Aquilante, F.; Malmqvist, P.-Å.; Pedersen, T. B.; Ghosh, A.; Roos, B. O., Cholesky decomposition-based multiconfiguration second-order perturbation theory (CD-CASPT2): application to the spin-state energetics of CoIII (diiminato)(NPh). *J. Chem. Theo. Comp.* **2008**, *4* (5), 694-702.
93. López-Alcalá, D.; Ruiz, A. M.; Baldoví, J. J., Exploring Spin-Phonon Coupling in Magnetic 2D Metal-Organic Frameworks. *Nanomaterials* **2023**, *13* (7), 1172.
94. Escalera-Moreno, L.; Suaud, N.; Gaita-Arino, A.; Coronado, E., Determining key local vibrations in the relaxation of molecular spin qubits and single-molecule magnets. *J. Phys. Chem. Lett.* **2017**, *8* (7), 1695-1700.
95. Iwahara, N.; Ungur, L.; Chibotaru, L. F., \tilde{J} -pseudospin states and the crystal field of cubic systems. *Phys. Rev. B* **2018**, *98* (5), 054436.
96. Iwahara, N.; Chibotaru, L. F., Exchange interaction between J multiplets. *Phys. Rev. B* **2015**, *91* (17), 174438.
97. Shrivastava, K., Theory of spin–lattice relaxation. *phys. stat. solid. (b)* **1983**, *117* (2), 437-458.

TOC: A detailed DFT and ab initio calculations unveil the correlation between spin-phonon vibrations and blocking temperature to provide design clues to improve the single-ion magnet characteristics in the pseudo- D_{5h} family of Dy(III) SMMs.

